ELSEVIER

Polymer 44 (2003) 1881–1892

polymer

www.elsevier.com/locate/polymer

Novel polyimide ionomers: CO_2 plasticization, morphology, and ion distribution

Andreas Taubert[a], John D. Wind[b], Donald R. Paul[b], William J. Koros[c,*], Karen I. Winey[a]

[a]*Department of Materials Science and Engineering, University of Pennsylvania, Philadelphia, PA 19104 USA*
[b]*Department of Chemical Engineering, University of Texas at Austin, Austin, TX 78712, USA*
[c]*School of Chemical Engineering, Georgia Institute of Technology, Atlanta, GA 30332, USA*

Received 10 September 2002; received in revised form 6 January 2003; accepted 8 January 2003

Abstract

Aluminum crosslinked 6FDA-6FpDA:DABA 2:1 and 1:2 copolyimide membranes were synthesized and their CO_2-induced plasticization was investigated. The membranes are unstable against CO_2 plasticization in long-term permeation tests at 40 atm CO_2 feed pressure at 35 °C. To correlate the plasticization with the polymer morphology, scanning transmission electron microscopy (STEM) was used to image the ionomers. STEM shows Al-rich aggregates in both ionomers, but the aggregate size and shape distribution in the 1:2 film is much more heterogeneous than in the 2:1. The 1:2 ionomer contains spherical aggregates with diameters from ~5 to 25 nm, chainlike assemblies of small spherical aggregates, vesicular aggregates, large distorted vesicular aggregates, and long band-like structures that extend up to 1000 nm in one dimension. The 2:1 ionomer only contains a few approximately spherical aggregates. Large fractions of both ionomers do not exhibit visible aggregates on the STEM length scale. IR spectroscopy reveals a neutralization level of the acid groups above 60% and transmission electron microscopy detects unreacted neutralizing agent in the polymer. Small angle and wide angle X-ray scattering patterns show scattering patterns that can be linked to the solid-state structure of the polymer backbone rather than the ionic aggregates.

Keywords: Polyimide ionomers; Aluminum crosslinking; CO_2 plasticization

1. Introduction

Polyimides have a broad range of applications from microelectronics to gas separation membranes. Many polyimides are insoluble in common solvents such as *N*-methyl-2-pyrrolidinone (NMP) and tetrahydrofuran (THF). Therefore, films or coatings are cast from the polyamic acid. This precursor polymer is then thermally imidized near 300 °C. However, the (4,4′-hexafluoroisopropylidene) diphthalic anhydride (6FDA) based polyimides tend to be soluble in common solvents due to the fluorine groups on the dianhydride moiety. As a result, these polyimides are attractive for applications such as the production of asymmetric hollow fiber gas separation membranes where high-temperature thermal treatments are problematic.

Various researchers have added metal salts and organometallic compounds to polyimides to improve their properties. Typically, the metal compound is added to a solution of the polyamic acid and this mixture is cast into a film. As the film is thermally cured at high temperatures, the metal ions react with the carboxylic acid groups of the polyamic acid. These ionomer structures are often complicated due to the competition of ring closure (i.e. conversion of polyamic acid to the polyimide) with acid group neutralization by the metal cations. Gel-formation during the coating process can also occur if the polyamic acid is crosslinked by the metal ions.

Cobalt and lithium chlorides have been added to 3,3′,4,4′-benzophenone tetracarboxylic dianhydride-4,4′-oxydianiline (BTDA-ODA) polyamic acids to improve the electrical conductivity; the surface conductivities increase, but the ion distribution depends on the processing conditions [1]. Improved adhesion at high temperatures and high humidity on flexible printed circuit boards was achieved by adding various metallic compounds and gelation inhibitors like acetylacetone to polyamic acids [2]. Silver salts were added to various polyamic acid

* Corresponding author. Tel.: +1-404-385-2684; fax: +1-404-385-2683.
E-mail address: wjk@che.gatech.edu (W.J. Koros).

0032-3861/03/$ - see front matter © 2003 Elsevier Science Ltd. All rights reserved.
doi:10.1016/S0032-3861(03)00052-1

solutions yielding ~75% reflectivity upon thermal imidization [3] or were infused into 3,3′,4,4′-biphenyltetracarboxylic dianhydride-4,4′-oxydianiline (BPDA-ODA) polyimides from supercritical CO_2, yielding surface reflectivities between 39 and 61% [4]. Adding metal compounds to BTDA-ODA polyamic acids and subsequent curing at 300 °C also improves their mechanical properties [5].

Polyimides also are attractive membrane materials for CO_2 removal from natural gas, propylene/propane separations, and aromatic/aliphatic separations by pervaporation. However, the separation performance at industrially relevant operating conditions is compromised by plasticization-induced permselectivity losses. Plasticization is an increase in the diffusivity of a penetrant due to the facilitation of local polymer segmental motion caused by the presence of another penetrant molecule [6]. Metal ion mediated crosslinking of acrylic and methacrylic acid-containing copolymers has been reported as a promising approach for controlling excessive swelling to maintain high permselectivity in hydrocarbon pervaporation [7,8]. However, in our studies, ionic crosslinking was not as effective as covalent crosslinking in suppressing plasticization in high-pressure CO_2/CH_4 separations [9].

Most previously reported synthetic procedures for polyimide ionomers involve high-temperature curing of the polyamic acid film because the resulting polyimide is insoluble. With our new technique, however, soluble 6FDA-based polyimides can be made by copolymerizing various amounts of 3,5-diaminobenzoic acid (DABA) into the polymer backbone [9,10]. Here, the carboxylic acid is a pendant group available for reaction with metal ions. The metal ions may be added to the polyimide solution as Al, Ag, Co, Cu, Pt, and other metal acetylacetonates. The resulting films do not need to be cured at high temperatures. With aluminum acetylacetonate ($Al(AcAc)_3$) gelation is not a problem, presumably because the acetylacetone inhibits this process [2]. Our synthetic procedure is therefore an attractive approach for making ionomer films with specific metal contents while retaining the rigid aromatic polyimide backbone that provides excellent mechanical properties.

Ionomers have complex morphologies with ion-rich domains ('aggregates') and ion-poor matrix regions. Typically, the aggregates are assumed to be spherical, monodisperse in size, and randomly distributed in the polymer matrix [11]. Small angle X-ray scattering (SAXS) is widely used to investigate the morphology of ionomers; several models have been used to fit the SAXS data and extract structural parameters. Most commonly, the typical ionomer scattering peak is fitted with the Yarusso–Cooper model [12,13] and aggregate radii, R_1, closest approach distances between two aggregates, R_{CA}, sample volumes per aggregate, v_P, and electron density differences, ρ, between the matrix and the aggregates are extracted from the fitting curve. Other experimental techniques used to investigate ionomers include dynamic mechanical analysis, EXAFS, infrared (IR) and nuclear magnetic resonance (NMR) spectroscopy. All these techniques have in common that to some extent they infer structural aspects from data fitting. In contrast, microscopy is a model-free technique that allows for the determination of the morphology above a certain length scale without data fitting.

Winey and coworkers have recently shown using scanning transmission electron microscopy (STEM) that the assumption of monodisperse spherical aggregates randomly distributed in a polymer matrix is only fulfilled in some cases [14,15]. Other ionomers exhibit aggregates with a variety of shapes, sizes, and different spatial distributions [16–19]. Furthermore, they have demonstrated by using X-ray energy dispersive spectroscopy (XEDS) that the matrix may contain a significant amount of metal-neutralized acid groups [19]. STEM imaging combined with XEDS, therefore, yields valuable information, which cannot be extracted from scattering or spectroscopy alone. As a result, STEM and atomic force microscopy (AFM) [20,21] are complementary to scattering and spectroscopy techniques.

Here we investigate the morphology of two Al-crosslinked ionomers 6FDA-6FpDA:DABA 2:1 and 1:2 using STEM, XEDS, WAXS, and SAXS. These polyimides have significantly different theoretical crosslinking densities and CO_2-induced plasticization behavior. The objective of this work is to compare the ionomer morphology with the CO_2 plasticization of the polymer by permeation and sorption characterization. In particular, we are interested to determine if CO_2 plasticization is related to the membrane morphology, specifically the ion distribution.

2. Experimental

2.1. Polymer synthesis and film preparation

Fig. 1 shows the polymer structure and the idealized crosslinking reaction. The polycondensation reaction was performed by the reaction of 6FDA, (4,4′-hexafluoroisopropylidene) dianiline (6FpDA), and 3,5-diaminobenzoic acid (DABA) in NMP followed by a chemical imidization with an equimolar mixture of triethylamine and acetic anhydride [22]. The uncrosslinked and Al-crosslinked films were prepared by casting filtered 2 wt% polyimide solutions containing 20% excess of the stoichiometric amount (with respect to the DABA content) of aluminum acetylacetonate ($Al(AcAc)_3$) in THF onto a Teflon casting dish. After solvent evaporation, the films were dried at 130 °C for 24 h under vacuum. We used a 20% excess of $Al(AcAc)_3$ to account for chain ends and insufficient polymer chain mobility for complete reaction. The 6FDA-6FpDA polymer without the DABA monomer was obtained from Hoechst-Celanese; it was cast from dichloromethane and dried in the same manner as the other films.

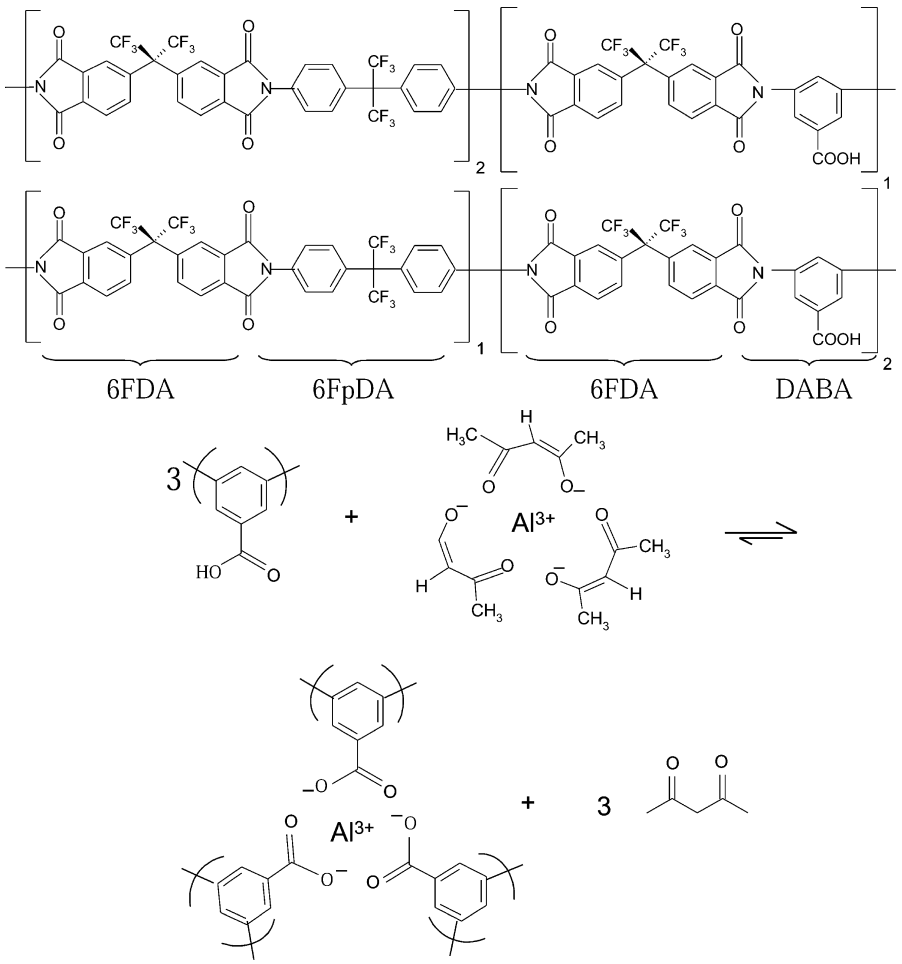

Fig. 1. Chemical structure of the copolymers and crosslinking reaction with $Al(AcAc)_3$.

2.2. Polymer characterization and gas transport measurements

IR spectra were recorded on a Nicolet Magnum 550 IR spectrometer with an N_2 purge. The conversion of $Al(AcAc)_3$ to aluminum carboxylate was estimated from Beer's law by taking the ratio of the peak intensity of the Al–O stretch of the acetylacetonate ion at 494 cm^{-1} (I_{494}) to that of the carbonyl bending of the aromatic imide bond at 725 cm^{-1} (I_{725}). This peak was used as the internal standard, since its intensity is invariant with the chemical treatment. This ratio is then normalized with the ratio (I_{494}/I_{725}) for a film of 6FDA-6FpDA (Hoechst-Celanese, no acid component) where a known concentration of $Al(AcAc)_3$ was added [23].

$$\text{Conversion} = 1 - \frac{(I_{494}/I_{725})_{\text{crosslinked 6FDA-6FpDA:DABA}}}{(I_{494}/I_{725})_{\text{6FDA-6FpDAw/same wt\% Al(AcAc)}_3}} \quad (1)$$

DSC thermograms were measured on a Perkin–Elmer DSC 7 with a heating rate of 20 °C/min under an N_2 purge. Gas permeation measurements were made by the constant volume/variable pressure technique [24] and CO_2 sorption measurements were made by the pressure decay method [25] at 35 °C. The gel fractions were determined by soaking the polymer films in THF for 5 days at 25 °C. The gelled films were dried at 100 °C under vacuum for 24 h and weighed to determine the gel fraction.

2.3. Electron microscopy and X-ray spectroscopy

The ionomers were stored under vacuum at room temperature at all times except for sample preparation purposes. Thin sections were prepared as follows: polystyrene (PS, $M_w \sim 250,000$ g/mol, Aldrich) was molded into ~300 μm thick films. A small piece of polyimide film was cut and deposited between two PS layers. The PS/sample/PS stack was compression molded for 5 min at ~1000 psi and ~107 °C. The sample embedded between the PS layers still had its original shape and sharp edges, indicating that no mixing between PS and ionomer occurred. Thin sections with nominal section thickness of 75 nm were microtomed at room temperature with a diamond knife, floated onto deionized water and collected on Mo support grids.

Both transmission electron microscopy (TEM) and STEM experiments were performed on a JEOL 2010F field emission electron microscope operated at 200 kV and equipped with a Princeton Gamma Tech (PGT) X-ray energy dispersive spectrometer, a Gatan bright field (BF), and a JEOL annular dark field (ADF) detector. For STEM experiments, a 50 μm condenser aperture, an ADF collection angle of ~40 mrad, and a 0.5 nm probe was used. The sample was maintained at a vacuum of $\sim 2 \times 10^{-5}$ Pa during all microscopy experiments. STEM magnifications ranged from 30,000 to 600,000 × and the image acquisition time was 21 s. The samples looked identical before and after STEM image acquisition, showing that the rastering electron beam does not measurably alter the microstructure of the material, even though some carbon contamination was observed. TEM experiments were made in the same microscope at 200 kV with a 150 μm condenser aperture, a 30 μm objective aperture, and a 20 μm diffraction aperture. TEM negatives were digitalized with an Agfa Duoscan T2500 at 2000 dpi. Image analysis was performed with Adobe Photoshop 5.0® using standard procedures, including background correction, gray level adjustments, and contrast enhancement.

X-ray Energy Dispersive Spectroscopy (XEDS) experiments were performed in the JEOL 2010F in STEM mode with a probe size of 1 nm to increase the signal to noise ratio. Spectra were acquired by rastering the electron beam over the sample in imaging mode for 5 min. Data analysis was performed with the IMIX software from PGT using the 'qualitative' acquisition mode: after background subtraction, the individual *K* lines of C, O, N, F, and Al from the sample and the Mo *M* lines from the grid were deconvoluted using IMIX routines and the integrated counts were recorded. Occasionally, Si *K* lines from the detector were also observed.

2.4. X-ray scattering

Small angle X-ray scattering (SAXS) experiments were performed on films in a q range from ~0.25 to 5.5 nm^{-1}, where q is the scattering vector ($q = 4\pi \times \sin\theta/\lambda$; where θ is the scattering angle and λ is the X-ray wavelength). In order to obtain reasonable scattering intensities, multiple polymer layers were assembled so that the total sample thickness was ~1 mm. These experiments utilized a previously described multiple angle X-ray scattering (MAXS) apparatus using Cu $K\alpha_1$ radiation ($\lambda = 1.5408$ Å) and a Bruker HiStar multiwire detector that provided highly sensitive area detection with very low dark current [19]. An integral vacuum was maintained between the generator and the detector, to reduce both attenuation and small-angle scattering by air and windows.

Wide angle X-ray scattering (WAXS) patterns of the polyimide films were obtained with a Philips APD 3520 diffractometer, Cu Kα source ($\lambda = 1.54$ Å). The apparatus scanned over the range 5–70°, with a dwell time of 3 s and a step size of 0.5°.

3. Results

3.1. Crosslinking density by infrared spectroscopy

The maximum crosslinking density is determined by the DABA content in the 6FDA-6FpDA:DABA polyimides. The actual crosslinking density may be lower and was established via IR spectroscopy. We used a 6FDA-6FpDA film with 12 wt% $Al(AcAc)_3$ to calibrate the IR spectra. Because 6FDA-6FpDA contains no carboxylic acids, there is no reaction of the acid groups of the polymer with the Al^{3+} cations; the film therefore allows the determination of the IR peaks associated with free $Al(AcAc)_3$ dispersed in the polymer matrix.

Fig. 2a shows the IR spectra of the 6FDA-6FpDA with and without dispersed $Al(AcAc)_3$. The peaks at 494 and 417 cm^{-1} are associated with the metal-oxygen vibrational modes of the acetylacetonate ion. They agree well with experimental [26] and theoretical data for pure $Al(AcAc)_3$ [27]. Fig. 2b and c are the IR spectra for the 6FDA-6FpDA:DABA 2:1 and 1:2 films, with and without aluminum. For the 2:1 film, the peaks at 494 and 417 cm^{-1} are barely visible, indicating that most of the aluminum is bonded to the carboxylate anions of the polymer. The spectra of the 6FDA-6FpDA:DABA 1:2 film show clear, but rather weak, peaks at 498 and 422 cm^{-1}, indicating residual unreacted $Al(AcAc)_3$ in the film.

Using Eq. (1), the conversion of the $Al(AcAc)_3$ is estimated to be 67% for the 2:1 and 52% for the 1:2 polyimide. The conversion calculation is based on the peak intensity and not the area, since the $Al(AcAc)_3$ peaks are not well resolved in the crosslinked ionomers. Because we used a 20% excess of neutralizing agent relative to the carboxylic acid content, full conversion of the carboxylic acid groups from the DABA moieties corresponds to an 83% conversion of the $Al(AcAc)_3$; therefore, the estimated DABA conversion is 80% for the 2:1 and 63% for the 1:2 polyimide. Therefore, the final crosslinking density of the 1:2 ionomer is 60% higher than that of the 2:1 ionomer.

The presence of unreacted $Al(AcAc)_3$ was further corroborated by TEM and electron diffraction experiments (data not shown). TEM bright field images revealed the presence of large (≥~ 0.5 μm) polygons that exhibited crystalline diffraction patterns. These particles are probably unreacted $Al(AcAc)_3$ trapped in the film. Due to the limited tilt range of the microscope we were unable to determine the crystallography of the particles.

3.2. Gel fractions in THF

The gel fraction of crosslinked polymers in a volatile solvent such as THF can also be used to describe the degree

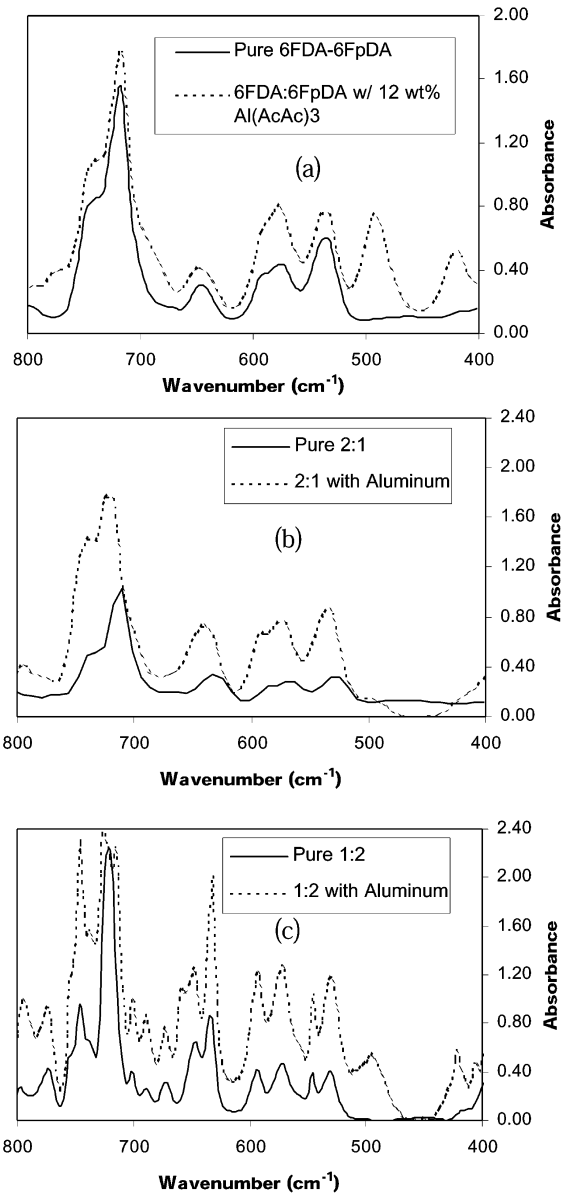

Fig. 2. IR spectra of polyimides as a function of aluminum and carboxylic acid content.

of crosslinking. The gel fractions of the 2:1 and 1:2 ionomer films were 77 and 93% after soaking in THF for 5 days at 25 °C, whereas the unneutralized films are completely soluble. The polymer in the 1:2 is essentially insoluble since much of the 7% that dissolves is likely to be unreacted $Al(AcAc)_3$. This shows that ionic crosslinking has a significant impact on the bulk solubility properties, but its impact on the CO_2-induced plasticization is far less pronounced (see below). The heterogeneity of the ion distribution described later may tend to promote plasticization, whereas the crosslinking should tend to suppress plasticization. We cannot make an unambiguous conclusion about these seemingly competitive forces from the given data, but the implication is that plasticization is more related to the local segmental mobility than to the bulk polymer properties such as gel fraction.

3.3. Glass transition temperatures

The unneutralized 2:1 and 1:2 films have glass transition temperatures of 322 and 327 °C, respectively. However, both Al-crosslinked polymers do not show a T_g when analyzed with DSC up to 450 °C, though there are some thermal events. In comparison, if the same 2:1 and 1:2 polyimides discussed here are covalently rather than ionically crosslinked, they show very little change in the T_g (< 10 °C) relative to the uncrosslinked precursor, but they have a significantly better resistance to CO_2 plasticization than the ionomers presented here and the uncrosslinked polymers [9]. Essentially no change in the T_g was observed for crosslinking of poly(methyl acrylate-*co*-acrylic acid)s with $Al(AcAc)_3$ via a similar procedure [8]. However, these polymers were much more flexible than the polyimides, with T_gs ~ 15–20 °C.

In other ionomers, multiple T_gs have been observed. They have been assigned to the glass transitions of the non-ionic polymer matrix and the ion-rich aggregates, respectively [28]. The presence of ionic groups in polymers has been shown to restrict the mobility of polymer chains compared to the non-ionic base resin [29,30]. It has been suggested that the chain rigidification effect is greater the more rigid the unneutralized polymer [11]. The absence of a T_g up to 450 °C in our samples implies that the polymer mobility is drastically reduced by the crosslinking, which normally would be advantageous for plasticization inhibition. However, this turns out not to be the case, as described below.

3.4. Permeation and sorption kinetics

For dense films with zero pressure on the downstream side of the membrane, the flux (n_A), normalized by the transmembrane partial pressure (Δp_A) and thickness (ℓ) is defined as the permeability ($\mathbf{P}_A$),

$$\mathbf{P}_A = n_A \frac{\ell}{\Delta p_A} \tag{2}$$

Permeability values are typically reported in Barrers

$$\left(1\ \text{Barrer} = 10^{-10}\ \frac{\text{cc(STP)cm}}{\text{cm}^2\ \text{cm Hg s}}\right).$$

According to the common solution–diffusion mechanism, the permeability can be written as the product of the diffusion coefficient, D, and the solubility coefficient, S

$$\mathbf{P}_A = D_A S_A \tag{3}$$

Fig. 3 shows that both the permeability and sorption increase over long time periods for both the crosslinked (i.e. ionomers) and uncrosslinked membranes. This is indicative of non-Fickian polymer relaxations due to CO_2

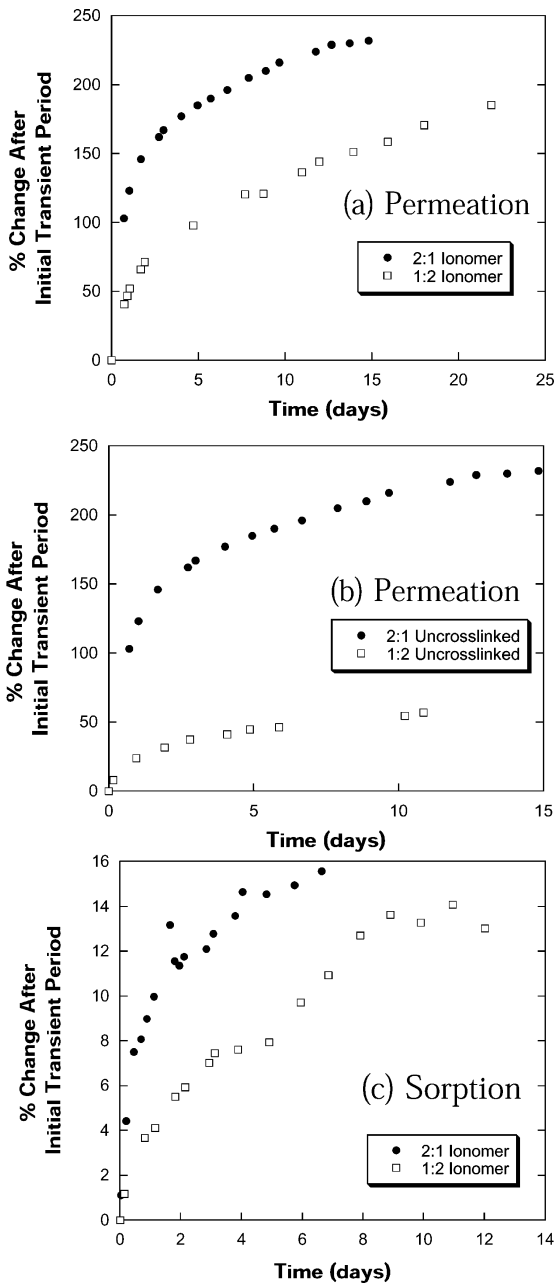

Fig. 3. Long-term permeation and sorption behavior for crosslinked and uncrosslinked membranes at 40 atm pure CO_2 and 35 °C.

plasticization, even though the sorption and permeation kinetics in membranes are frequently described by standard Fickian models. For Fickian sorption, the permeation time lag (θ) or time to reach steady-state is

$$\theta = \frac{\ell^2}{6D} \tag{4}$$

where ℓ is the membrane thickness and D is the average diffusion coefficient of the penetrant in the membrane. The time to reach half of the equilibrium sorption level is [6]

$$t_{1/2} = 0.0492\frac{\ell^2}{D} \tag{5}$$

For Fickian sorption uptake, equilibrium is typically reached within six 'half-time' periods. For all of the samples considered here, sorption and permeation equilibrium times based on Fickian models are less than 15 min.

However, because our membranes are plasticized, there is a relaxation-controlled time-dependent function superimposed onto the Fickian transient functions to describe the sorption and diffusion behavior [31,32]. Permeability is the product of the sorption and diffusion coefficients, and Fig. 3a shows that diffusion is much more affected by the plasticization than sorption (Fig. 3c) for both ionomers. Interestingly, the 1:2 ionomer shows much greater long-term increases in the permeability (or diffusion coefficient) than the uncrosslinked membrane. This is in stark contrast to the solubility behavior in THF, where the unneutralized samples are completely soluble and the ionomers have significant gel fractions. Table 1 shows the permeability, diffusion, and sorption coefficients for each membrane.

Therefore, even though IR spectroscopy shows significant crosslinking, ionic crosslinking is much less effective in suppressing CO_2 plasticization in our polyimide membranes than covalent crosslinking of the same precursor polymers [9]. The sorption and permeation data suggest that the polymer morphology may be different, thereby giving rise to the observed sorption and permeation behavior. In the following sections, we characterize the ionomer morphology with STEM and XEDS to confirm the presence of different morphologies in the two ionomers.

3.5. Scanning transmission electron microscopy and X-ray spectroscopy

Fig. 4 is a STEM bright field (BF)/annular dark field (ADF) image pair of the Al-crosslinked 1:2 ionomer. The BF image shows dark features of various shapes and sizes in a bright matrix. The corresponding ADF image shows a contrast reversal where the dark features in the BF images appear bright and the bright matrix appears dark. This behavior indicates that the isolated features contain elements with a higher atomic number Z in a lower Z matrix. Because the Rutherford scattering power of an element scales approximately with Z^2 [33–35], the Al^{3+} ($Z = 13$) ions in the ionic aggregates scatter more electrons into the annular dark field detector than the polymer matrix, which consists of carbon ($Z = 6$), nitrogen ($Z = 7$), oxygen ($Z = 8$), and fluorine ($Z = 9$). As a result, the Al-rich aggregates appear bright in STEM ADF and dark in the STEM BF images. Fig. 4 also shows that there are rather large regions without visible aggregates on the STEM length scale (STEM resolution is ~1 nm).

Fig. 5 shows that the Al-rich aggregates in the 1:2 ionomer vary in size and shape. While some aggregates are spherical and rather small (~5 nm), others are on the order of ~25 nm in diameter and resemble the vesicular structures previously observed in Zn-neutralized sulfonated poly(styrene) (Zn-SPS) [16,17] and Cs-neutralized poly-

Table 1
CO_2 sorption and transport properties at 10 atm and 35 °C

Polymer	Permeability (Barrers)	Sorption coefficient (cm^3(STP)/(cm^3 atm))	Diffusion coefficient (cm^2/s)
2:1 Uncrosslinked	29	4.2	5.2×10^{-8}
2:1 Ionomer	25	4.0	4.8×10^{-8}
1:2 Uncrosslinked	17	3.7	3.5×10^{-8}
1:2 Ionomer	19	4.2	3.4×10^{-8}

(styrene-ran-methacrylic acid) (Cs-SMAA) [18]. Chainlike assemblies of small spherical aggregates and even extended structures similar to large distorted vesicles and long band-like structures exist in the same sample. This current paper reports for the first time chainlike and large, extended ion rich aggregates via STEM. Contrast reversal of all dark features occurs between the BF and ADF images suggesting that these structures are Al-rich ionic domains.

Fig. 6a is a typical image of the 2:1 ionomer and shows that this ionomer is much more homogeneous than the 1:2 ionomer. Large fractions of the material do not exhibit visible aggregates on the STEM length scale. Fig. 6b shows that some aggregates are still present, but no extended structures resembling the chain-like ion-rich domains in the 1:2 sample. Images with magnifications up to 600,000 × confirm the absence of small aggregates on the STEM length scale.

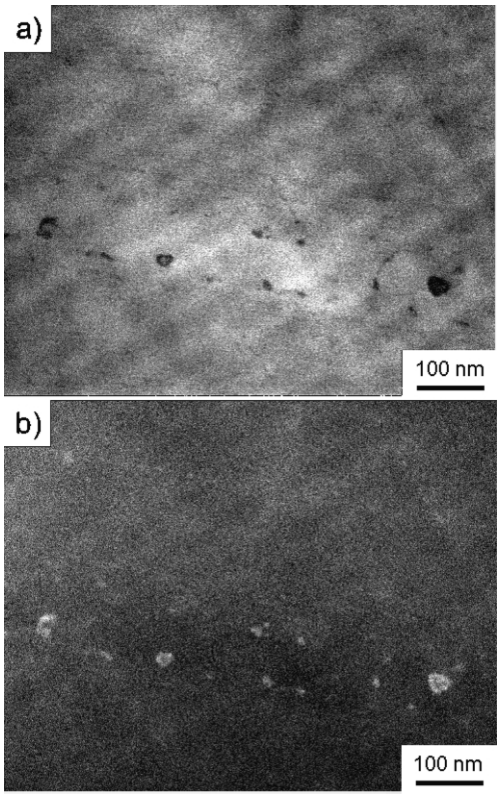

Fig. 4. STEM BF (a) and ADF (b) image of Al-rich aggregates in the 1:2 Al-crosslinked polyimide ionomer. Contrast reversal confirms that they are Al-rich. The slight contrast variation in the image background is most likely due to sample preparation.

We collected X-ray energy dispersive (XEDS) spectra that probe ~2.5 μm^2 area of the microtomed section. A typical spectrum is shown in Fig. 7. The integrated Al *K* X-ray counts of these spectra exhibit large differences. Some regions exhibit intense Al *K* lines (~14,000 counts), whereas other areas barely show any signal (~300 counts). This observed increase in the Al signal correlates with a higher density of aggregates. However, we also detected weak Al *K* lines in the absence of aggregates. The presence of N, O, and F *K* lines along with the Al *K* line clearly confirms that we are probing the ionomer and not erroneously the polystyrene used to stabilize the polyimides.

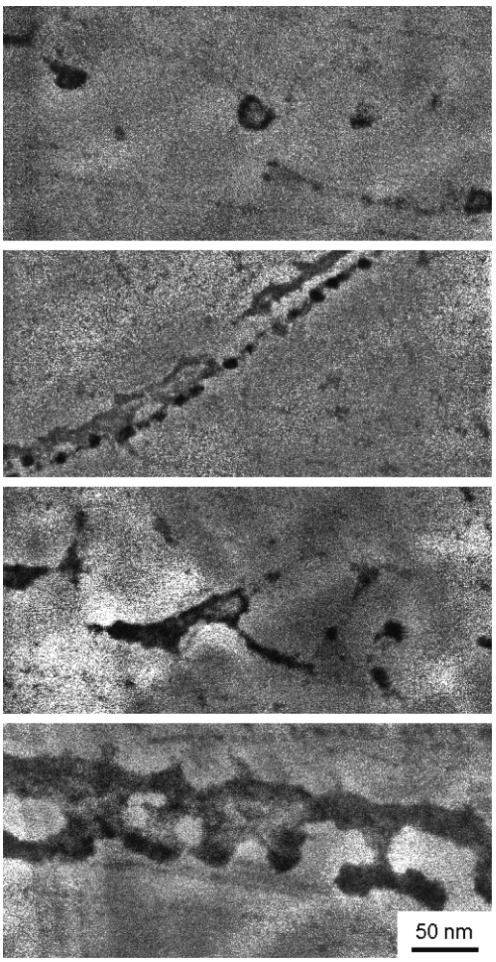

Fig. 5. STEM BF images of various aggregates in the Al-neutralized 1:2 ionomer. The aggregates have irregular shapes and various sizes. The slight contrast variation in the image background is most likely due to sample preparation.

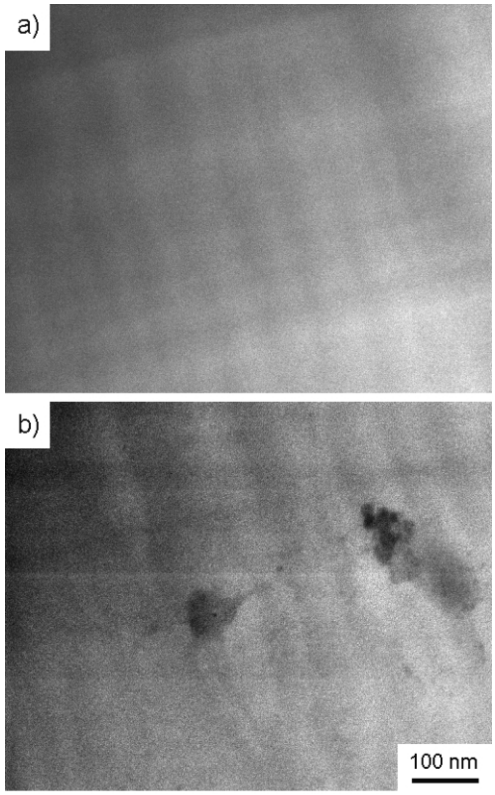

Fig. 6. STEM BF images of the 2:1 Al-crosslinked polyimide ionomer. Most of the material does not exhibit any aggregates on the STEM length scale (a) but some aggregates are visible (b). The slight contrast variation in the image background is most likely due to sample preparation.

The XEDS spectra confirm that the aggregates observed by STEM are Al-rich because the Al *K* line intensity correlates with the presence of aggregates, but it also shows the presence of Al in the matrix, either as isolated groups or as aggregates too small for the STEM to resolve.

A quantification of the XEDS data is difficult for several reasons. First, we cannot tilt the sample enough to fully determine the 3D shape of the ionic aggregates. If the aggregate is spherical, we can calculate how much of the probed volume is aggregate and how much is surrounding

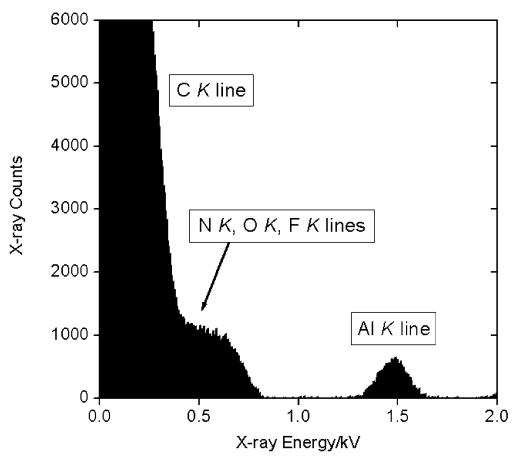

Fig. 7. XEDS spectrum of the 1:2 Al-crosslinked polyimide ionomer.

matrix and we can quantify these data by acquiring spectra from regions with and without aggregates. If, however, the aggregate shape is unknown, the contributions from the aggregate and matrix cannot be separated. For example, the aggregates in Fig. 5 may span only a fraction of the section (Fig. 8b) or the whole section thickness (Fig. 8c), which will affect data analysis.

Second, we could use the N or O *K* line intensity to determine the ratio of Al to N or O. However, both the N and O *K* line intensities are small and overlap with the F and C *K* lines at the lower end of the X-ray spectra. Neither the acid group nor the acetylacetonate ion contains unique elements relative to the bulk polymer that would enable the determination of the aggregate composition (free $Al(AcAc)_3$ versus Al(COO)). Moreover, the F *K* line intensity cannot be quantified because the C–F bond is unstable against electron beam irradiation [36]. We currently do not have an estimate of how much F is lost over the entire acquisition time.

3.6. Small and wide angle X-ray scattering

Fig. 9 shows the SAXS patterns of the unneutralized precursor polymers and the neutralized 1:2 and 2:1 ionomers along with the patterns of the 6FDA-6FpDA polymer both with and without $Al(AcAc)_3$. All patterns exhibit a small peak at $q \sim 3.3\ nm^{-1}$ and only the pattern of the 1:2 crosslinked ionomer exhibits a tiny second peak at $\sim 4.4\ nm^{-1}$. The position of these peaks is higher than many ionomers reported in the literature, although Kutsumizu et al. reported SAXS peaks at $3–4\ nm^{-1}$ for non-crystalline ethylene ionomers [29]. The peak is weakest for the pure 6FDA-6FpDA. Also, the pattern of the unneutralized 2:1 copolymer shows a weak shoulder at $\sim 1.1\ nm^{-1}$. The peak observed for the 6FDA-6FpDA with $Al(AcAc)_3$ is broader than the other peaks, the implications of which will be discussed below. The position, shape, and intensity of the observed scattering peaks our six copolymers does not change regardless of the fact that two samples are not neutralized and that the samples vary in their chemical composition, in particular in their acid concentration. This is in contrast to the STEM images that reveal distinct differences between the two neutralized ionomers.

Fig. 10 shows the respective WAXS patterns. The patterns of both the neutralized and the unneutralized polyimides show an intense peak at $2\theta \sim 16°$ and a second

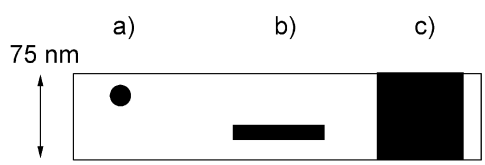

Fig. 8. Schematic of a cross-sectional view of a STEM sample depicting different possibilities of aggregate locations in the thin section. The aggregates in b and c are highly simplified presentations of the large structures shown in Fig. 5.

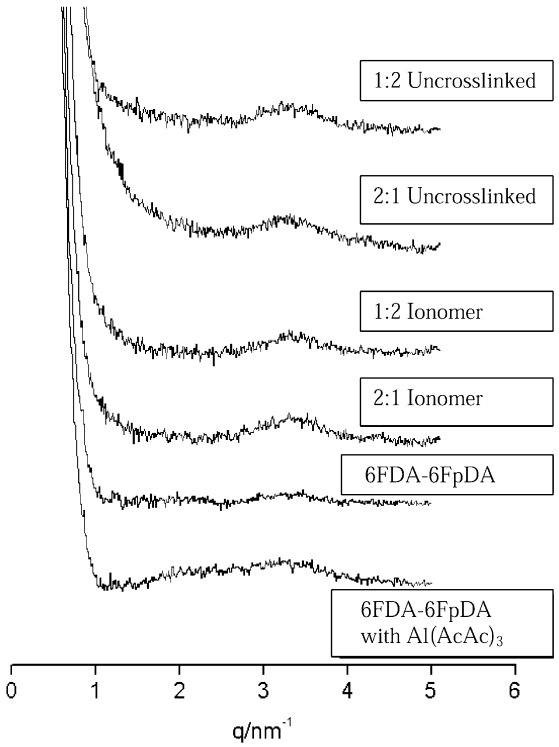

Fig. 9. SAXS patterns of the unneutralized and neutralized 1:2 and 2:1 copolymers and for 6FDA-6FpDA, pure and with $Al(AcAc)_3$. The unneutralized 2:1 copolymer exhibits a weak shoulder at $q \sim 1.1\ nm^{-1}$ and 6FDA-6FpDA with $Al(AcAc)_3$ exhibits a broader peak at $\sim 3\ nm^{-1}$ compared to the other polymers.

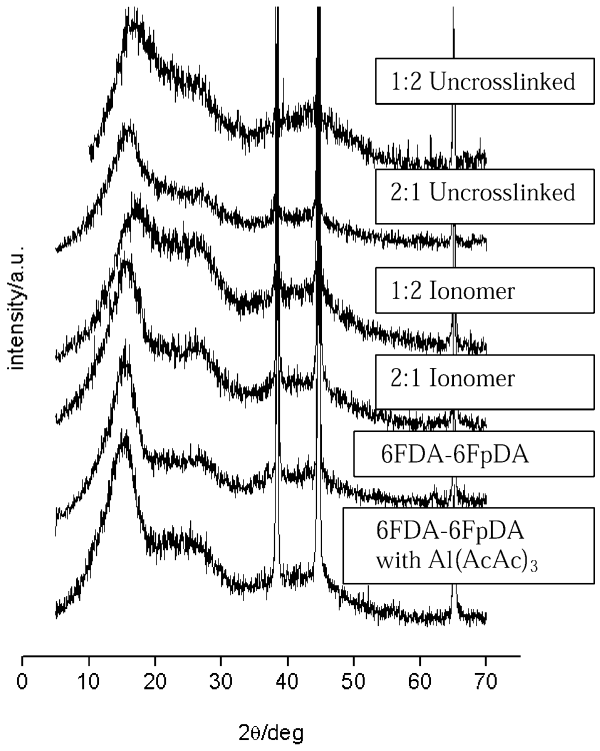

Fig. 10. WAXS patterns of the following the unneutralized and neutralized 1:2 and 2:1 copolymers and for 6FDA-6FpDA without and with $Al(AcAc)_3$. The sharp reflections at 38.5, 44.6, and 65.2 2θ/deg are from the aluminum sample holder.

peak at $2\theta \sim 26°$. These peaks are also visible in the patterns of the pure 6FDA-6FpDA and of the 6FDA-6FpDA containing $Al(AcAc)_3$. The *d*-spacing corresponding to the main peak in the amorphous polyimides is believed to correspond to the average inter-chain spacing [37] and correlates with the gas permeability at low feed pressures [38].

Both the peak positions and the intensities in the SAXS and WAXS patterns are similar to X-ray scattering data reported earlier on polyamic acids and polyimides [39]. These authors found several peaks with characteristic intensities and *d*-spacings: a sharp peak of medium intensity ($d \sim 1.5$ nm), an intense peak ($d \sim 0.46$ nm), a less intense peak or shoulder ($d \sim 0.33$ nm), and a series of smaller peaks with $d \sim 0.24$, 0.20, and 0.11 nm; the authors explained these patterns with a smectic, liquid crystalline-like structure. The peaks observed in the WAXS patterns are at ~0.55 and 0.34 nm. The peak observed in SAXS corresponds to a d-spacing ~19 nm, but there is no periodicity of ionic aggregates on this length scale, as shown by STEM. These results imply that the SAXS and WAXS peaks are due to the polyimide and *not* to the presence of an ionic structure, particularly because the same type of scattering patterns were observed for the unneutralized materials and also for 6FDA-6FpDA with and without $Al(AcAc)_3$. This is in contrast to the behavior of block copolymers, where the correlation between SAXS patterns and morphology is well understood.

4. Discussion

Ion-rich aggregates are dark in STEM BF and bright in STEM ADF images because STEM is based on atomic number contrast. The contrast reversal observed here therefore implies that the features in the STEM images of the Al-neutralized polyimide ionomers are Al-rich ionic domains that form in a polymer matrix with a lower average atomic number. This is further supported by X-ray spectra acquired from ~2.5 μm^2 areas because the Al *K* lines are more intense in the presence of many aggregates.

STEM images reveal distinct variations in the morphologies of the two Al-neutralized ionomers. The 1:2 ionomer has a complex morphology with aggregates that have a range of shapes, sizes, and a heterogeneous spatial distribution. Aggregate shapes include isolated spheres, vesicular aggregates, chains of spheres, and large features that extend up to 1000 nm in length. Furthermore, the aggregate number density varies within one sample: some regions have a high aggregate concentration while others are largely depleted of aggregates visible with STEM. In contrast, to the 1:2 ionomer, the 2:1 ionomer only exhibits few and widely separated ion-rich aggregates; here, the distance between aggregates is on the order of hundreds of nanometers up to several micrometers.

These polyimide ionomers share some similarities with

other ionomers that have been analyzed with STEM: (1) the polyimide ionomers presented here exhibit ion-rich aggregates in STEM. Naturally, the presence of ionic aggregates is expected because the charged carboxylate groups and the Al cations will attract one another and phase-separate from the relatively non-polar polyimide matrix. However, Taubert and Winey have also observed that a Na-neutralized poly(ethylene-ran-methacrylic acid) (Na-EMAA) ionomer did not exhibit aggregates on the STEM length scale of ~1 nm [19], which is similar to some areas in the 1:2 and to the majority of the 2:1 ionomer presented here. (2) The 1:2 ionomer contains spherical and vesicular aggregates that resemble aggregates observed before in polystyrene based ionomers. (3) Similar to observations on Zn-neutralized sulfonated polystyrene (Zn-SPS) and a Na-EMAA ionomer, the 1:2 ionomer exhibits some degree of macrophase separation.

However, there are two main differences between the ionomers presented here and Zn-SPS and Na-EMAA: (1) the 1:2 ionomer exhibits large chain-like and extended ion-rich domains. These have never been observed before and thus further broaden the range of shapes observed in ion-rich aggregates. (2) The boundaries between aggregate-rich and aggregate-poor regions in the macrophase-separated Zn-SPS and Na-EMAA are fairly sharp [16–19]. In contrast, the boundaries between aggregate-rich and aggregate-deficient regions in the 1:2 polyimide presented here exhibit a smooth transition.

The differences between the polyimide ionomers and other systems may be due to the high glass transition temperatures of the precursor polyimides. The glass transitions of the precursor polymers occur well over 300 °C. In contrast, polystyrene has a T_g of approximately 100 °C and the T_g of polyethylene is around −50 °C. This is significant, because the polyimide ionomers presented here are made by solution casting followed by annealing under vacuum *below* the T_g of the polyimide. In contrast, polystyrene ionomers are usually neutralized via a solution process and polyethylene ionomers are made by melt neutralization well above the T_g. While some neutralization of the polyimides may occur during solution casting, it may not be terminated. Once the films are cast, the polymer chains are much less flexible, which may slow down the neutralization process during annealing. It may also impede the formation of an equilibrium structure and 'freeze' the as-cast non-equilibrium structure. If the observed heterogeneity in the 1:2 morphology was a non-equilibrium structure only due to a high T_g, however, we would expect to observe it in both ionomers, because their T_gs only differ by a few degrees and their solution casting times and conditions were identical. We therefore believe that the amount of crosslinks also affects the morphology, as we will discuss now.

The morphological differences between the 1:2 and the 2:1 ionomers may arise from: (1) precipitation and trapping of $Al(AcAc)_3$ within the polymer or (2) differences in carboxylic acid and aluminum ion concentrations and crosslinking density. We have shown using IR spectroscopy that the crosslinking density in the 1:2 ionomer is ~60% higher than in the 2:1 ionomer. A non-equilibrium structure in the 1:2 ionomer may therefore most likely originate in the combination of the high T_g with the higher acid concentration of the 1:2 precursor polymer. The higher crosslinking leads to lower chain mobility and prevents the formation of an equilibrium morphology. Also, the lower crosslinking density in the 2:1 ionomer may allow the neutralizing agent to diffuse in the sample more freely, which may lead to a more homogeneous neutralization during solution casting and also during annealing and, hence lead to a more homogeneous morphology.

Precipitation of $Al(AcAc)_3$ may lead to regions containing trapped neutralizing agent. We believe that this is of minor importance though, because, with only one exception in the 1:2 ionomer, electron diffraction did not reveal any crystallinity within either sample, where the only crystalline material is solid $Al(AcAc)_3$. Also, the IR spectra of the 1:2 ionomer only show a weak signal assigned to trapped neutralizing agent, and the peak for the $Al(AcAc)_3$ in the 2:1 ionomer was negligible. We thus conclude that precipitation of neutralizing agent may contribute to the heterogeneity in the 1:2 ionomer, but is not the major cause for the observed heterogeneity, nor is it the origin of the isolated features observed in the 2:1 ionomer.

The above-introduced arguments are further supported by molecular modeling experiments. We used HyperChem 7.0® from Hypercube, Inc., with simple bond angle constraints, to calculate the DABA spacing for an extended chain: the DABA spacing is 2.5 and 1.8 nm for the 2:1 and 1:2 polymers, respectively. In contrast, the ionic aggregates in the 1:2 ionomer range in size from 5 to >1000 nm. Many aggregates are separated by more than 100 nm from each other. This spacing is much greater than the calculated DABA spacing, which supports our arguments above because it suggests that there are multiple DABA groups from many polymer chains participating in the aggregates. This will in turn limit the flexibility of adjacent segments that may contain acid groups: even if these acid groups are neutralized, they cannot move freely enough to form an aggregate or an aggregate with an energetically favorable shape. They, therefore, become immobilized by the neighboring ionic groups that are already aggregated. This may lead to the very heterogeneous morphology of the 1:2 ionomer, which has a higher acid fraction than the 2:1 ionomer. The polymer between the aggregates may be uniformly crosslinked, especially for the 2:1 polymer, where few aggregates are seen in the STEM images.

Aside from the Al-rich aggregates, there is evidence from XEDS that the matrix also contains Al. The Al dispersed in the matrix could be isolated $Al(COO)_3$ or aggregates that are too small for the STEM to resolve (i.e. below ~1 nm). A structure containing a significant number of cations in the matrix is consistent with STEM and XEDS results on a Na-neutralized poly(ethylene-ran-methacrylic acid) ionomer

[19]. It is also consistent with ^{23}Na solid-state NMR (SSNMR) studies by O'Connell et al. [40–43] on Na-neutralized SPS. These authors explain the appearance of two different signals in the NMR spectra with the presence of isolated metal ion sites in the polystyrene matrix and aggregated Na-neutralized acid groups. O'Connell et al. assign this broad peak to variations in the local cation environment due to dimers, trimers, etc., suggesting a heterogeneous structure of the cation environment. This is qualitatively consistent with the STEM and XEDS data presented here, even though the ionomers are very different.

Despite the structural differences, both membranes plasticize at high CO_2 pressures. Plasticization may occur due to a weakening of the ionic bond by solvation effects of the quadrupolar CO_2 molecules. It does not appear that heterogeneity in the ion distribution has anything to do with CO_2 plasticization in membrane processes, since the 2:1 and 1:2 both plasticize significantly. The length scales associated with the polymer chain volume fluctuations that control small molecule diffusion are likely to be smaller than the nm-length scale observed in STEM. However, the morphology on the nanometer length scale probably has a direct impact on the Angstrom scale motions that govern CO_2 diffusion through the membrane because the crosslinking density defines the size of the flexible chains in the membrane and so controls the diffusion of the penetrant. This paper demonstrates that the effects of crosslinking density and aggregate formation may affect the membrane performance in a more complex manner than originally thought. Since plasticization is related to the segmental mobility, it is likely that a uniformly crosslinked polymer is preferred to limit the segmental mobility uniformly throughout the polymer. The natural tendency for ions to aggregate makes this uniformity inherently less attainable than with covalent crosslinking agents.

Changes in the ionomer preparation procedure could change the ionomer morphology and produce more stable membranes. The solvent evaporation rate and the film formation and/or annealing temperature could be varied or the partially crosslinked films could be swollen in a strong solvent to facilitate the mobility necessary for complete neutralization. Additionally, the metal ion in the acetylacetonate compound may affect the morphology and the final crosslinking degree.

5. Conclusions

A novel crosslinking method to produce polyimide ionomers with a controlled carboxylic acid content and crosslinking degree has been developed. These ionomers can be crosslinked at low temperatures and gel formation is inhibited during the casting procedure. IR spectroscopy shows a crosslinking conversion above 60% for both ionomers. The CO_2-induced plasticization in high-pressure permeation leads to unstable membrane performance over long-term operating periods. The 6FDA-6FpDA:DABA 1:2 ionomer exhibits Al-rich aggregates of various sizes and shapes, with a very heterogeneous spatial distribution. The 2:1 ionomer is much more homogeneous and only shows a few aggregates on the STEM length scale. XEDS found a strong correlation between the Al *K* line intensity in the XEDS spectra and the aggregate numbers. IR and TEM show evidence of unreacted neutralizing agent in the ionomers. The comparison of the STEM and XEDS data with the permeation results suggests that the performance of these materials is much more dependent on the Angstrom-level motions of polymer chain segments than on the morphology on a nanometer-level as revealed by STEM.

Acknowledgements

This research has been supported by United States Department of Energy grant DE-FG03-95ER14538 at the University of Texas at Austin and NSF-DMR grant 99-06829 and the Petroleum Research Foundation grant 34038-AC7 at the University of Pennsylvania.

References

[1] Rancourt JD, Taylor LT. Macromolecules 1987;20(4):790–5.
[2] Ono K, Nishinaka M, Akahori R. US Patent 6,207,739, Kanegafuchi Chemical Industry Co., Ltd., Japan; 1999.
[3] Thompson DW, Caplan ML, St. Clair AK. US Patent 5,677,418, United States National Aeronautics and Space Administration, USA; 1997.
[4] Rosolovsky J, Boggess RK, Rubira AF, Taylor LT, Stoakley DM, St. Clair AK. J Mater Res 1997;12(11):3127–33.
[5] St. Clair AK, Taylor LT. J Appl Polym Sci 1983;28:2393–400.
[6] Koros WJ, Hellums MW. Encycl Polym Sci Engng 1990;724–802.
[7] Inui K, Noguchi T, Miyata T, Uragami T. J Appl Polym Sci 1999; 71(2):233–41.
[8] Matsui S, Paul DR. J Membr Sci 2002;195(2):229–45.
[9] Wind JD, Staudt-Bickel C, Paul DR, Koros WJ. Ind Engng Chem Res 2002;41(24):6139–48.
[10] Staudt-Bickel C, Koros WJ. J Membr Sci 1999;155(1):145–54.
[11] Eisenberg A, Hird B, Moore RB. Macromolecules 1990;23(18): 4098–107.
[12] Yarusso DJ, Cooper SL. Macromolecules 1983;16(12):1871–80.
[13] Yarusso DJ, Cooper SL. Polymer 1985;26(3):371–8.
[14] Winey KI, Laurer JH, Kirkmeyer BP. Macromolecules 2000;33(2): 507–13.
[15] Laurer JH, Winey KI. Macromolecules 1998;31(25):9106–8.
[16] Kirkmeyer BP, Winey KI, Weiss RA. Microsc Microanal 2000;6(2): 1112–3.
[17] Kirkmeyer BP, Weiss RA, Winey KI. J Polym Sci: Polym Phys Ed 2001;39(5):477–83.
[18] Kirkmeyer BP, Taubert A, Kim JS, Winey KI. Macromolecules 2002; 35(7):2648–53.
[19] Taubert A, Winey KI. Macromolecules 2002;35(19):7419–26.
[20] McLean RS, Doyle M, Sauer BB. Macromolecules 2000;33(17): 6541–50.
[21] Sauer BB, McLean RS. Macromolecules 2000;33(21):7939–49.
[22] Husk GR, Cassidy PE, Gebert KL. Macromolecules 1988;21(5): 1234–8.

[23] Conley RT. Infrared spectroscopy, 2nd ed. Boston: Allyn and Bacon; 1972.
[24] O'Brien KC, Koros WJ, Barbari TA, Sanders ES. J Membr Sci 1986; 29(3):229–38.
[25] Koros WJ, Paul DR. J Polym Sci: Polym Phys Ed 1976;14:1903–7.
[26] Dismukes JP, Jones LH, Bailar Jr JC. J Phys Chem 1961;65792–5.
[27] Diaz-Acosta I, Baker J, Cordes W, Pulay P. J Phys Chem A 2001; 105(1):238–44.
[28] Eisenberg A, Kim J-S. Introduction to ionomers. New York: Wiley; 1998.
[29] Kutsumizu S, Tadano K, Matsuda Y, Goto M, Tachino H, Hara H, Hirasawa E, Tagawa H, Muroga Y, Yano S. Macromolecules 2000; 33(24):9044–53.
[30] MacKnight WJ, McKenna LW, Read BE. J Appl Phys 1967;38(11): 4208–12.
[31] Berens AR, Hopfenberg HB. Polymer 1978;19(5):489–96.
[32] Wessling M, Huisman I, Boomgaard Tvd, Smolders CA. J Polym Sci: Polym Phys Ed 1995;33(9):1371–84.
[33] Pennycook SJ. Ultramicroscopy 1989;30(1-2):58–69.
[34] Williams CE, Colliex C, Horrion J, Jerome R. ACS Symp Ser 1989; 395:439–44.
[35] Williams DB, Carter CE. Transmission electron microscopy—a textbook for materials science. New York: Plenum Press; 1996.
[36] Lieser G, Schmid SC, Wegner G. J Microsc-Oxford 1996;18:353–9.
[37] Schwartz LH, Cohen HB. Diffraction from materials. New York: Academic Press; 1977.
[38] Kim TH, Koros WJ, Husk GR, O'Brien KC. J Membr Sci 1988;37: 45–62.
[39] Takahashi N, Yoon DY, Parrish W. Macromolecules 1984;17(12): 2583–8.
[40] O'Connell EM, Root TW, Cooper SL. Macromolecules 1994;27(20): 5803–10.
[41] O'Connell EM, Root TW, Cooper SL. Macromolecules 1995;28(11): 3995–9.
[42] O'Connell EM, Root TW, Cooper SL. Macromolecules 1995;28(11): 4000–6.
[43] O'Connell EM, Peiffer DG, Root TW, Cooper SL. Macromolecules 1996;29(6):2124–30.